remote sensing

MDPI

Article

Modeling the Effects of Global and Diffuse Radiation on Terrestrial Gross Primary Productivity in China Based on a Two-Leaf Light Use Efficiency Model

Yanlian Zhou [1], Xiaocui Wu [2], Weimin Ju [3,*], Leiming Zhang [4], Zhi Chen [4], Wei He [3], Yibo Liu [5] and Yang Shen [3]

1 School of Geography and Ocean Science, Nanjing University, Nanjing 210023, China; zhouyl@nju.edu.cn
2 Department of Microbiology and Plant Biology, Center for Spatial Analysis, University of Oklahoma, Norman, OK 73019, USA; xiaocui.wu@ou.edu
3 International Institute for Earth System Science, Nanjing University, Nanjing 210023, China; weihe@nju.edu.cn (W.H.); y_shen@yeah.net (Y.S.)
4 Synthesis Research Center of Chinese Ecosystem Research Network, and Key Laboratory of Ecosystem Network Observation and Modeling, Institute of Geographic Sciences and Natural Resources Research, Chinese Academy of Sciences, Beijing 100101, China; zhanglm@igsnrr.ac.cn (L.Z.); chenz@igsnrr.ac.cn (Z.C.)
5 Jiangsu Key Laboratory of Agricultural Meteorology, School of Applied Meteorology, Nanjing University of Information Science and Technology, Nanjing 210044, China; yiboliu@nuist.edu.cn
* Correspondence: juweimin@nju.edu.cn

Received: 25 August 2020; Accepted: 7 October 2020; Published: 14 October 2020

Abstract: Solar radiation significantly affects terrestrial gross primary productivity (GPP). However, the relationship between GPP and solar radiation is nonlinear because it is affected by diffuse radiation. Solar radiation has undergone a shift from darker to brighter values over the past 30 years in China. However, the effects on GPP of variation in solar radiation because of changes in diffuse radiation are unclear. In this study, national global radiation in conjunction with other meteorological data and remotely sensed data were used as input into a two-leaf light use efficiency model (TL-LUE) that simulated GPP separately for sunlit and shaded leaves for the period from 1981 to 2012. The results showed that the nationwide annual global radiation experienced a significant reduction (2.18 MJ m^{-2} y^{-1}; $p < 0.05$) from 1981 to 2012, decreasing by 1.3% over this 32-year interval. However, the nationwide annual diffuse radiation increased significantly ($p < 0.05$). The reduction in global radiation from 1981 to 2012 decreased the average annual GPP of terrestrial ecosystems in China by 0.09 Pg C y^{-1}, whereas the gain in diffuse radiation from 1981 to 2012 increased the average annual GPP in China by about 50%. Therefore, the increase in canopy light use efficiency under higher diffuse radiation only partially offsets the loss of GPP caused by lower global radiation.

Keywords: GPP; diffuse radiation; global radiation; TL-LUE

1. Introduction

Carbon sequestration is extremely important for global change studies [1]. Terrestrial gross primary productivity (GPP), which indicates the ability of vegetation to use light energy through fixation of carbon dioxide during photosynthesis, is a primary component of the terrestrial carbon cycle [2]. Solar radiation substantially affects the ecosystem GPP [3].

Global radiation (R_g) includes both direct and diffuse components. Compared with direct radiation, diffuse radiation (R_d) is more readily distributed evenly in the canopy and shows higher photosynthetic saturation. Therefore, higher R_d increases the canopy light use efficiency (LUE) and

thus leads to the enhancement of GPP [4–7]. Consequently, under cloudy or severe haze conditions, even if R_g decreased, vegetation GPP can increase as a result of the higher R_d component.

Many studies have quantitatively or mechanistically assessed the influence of changes in R_d on GPP at the site scale. An increase in R_d results in enhanced canopy LUE and hence leads to an increase in vegetation productivity. For example, Gu et al. [8] confirmed that canopy LUE under R_d was higher than that under direct radiation for six vegetation types. Gu et al. [9] observed that after a volcanic eruption, changes in R_d on the GPP of Harvard Forest increased by 3–21% because of the increase in the diffuse radiation fraction.

Previous studies have evaluated the effects of R_d on GPP at the regional scale with ecological models. Black et al. [10] investigated the impact of radiation on GPP over the past 50 years. The effect was greater for agricultural lands and grasslands than for forests, as demonstrated by flux data. Mercado et al. [5] observed that the reduction in global photosynthetically active radiation (PAR) reduced global terrestrial carbon sinks by 14.4%, whereas an increase in R_d increased global terrestrial carbon sinks by 9.3%. Chen et al. [11] coupled a terrestrial ecological model and an atmospheric radiation transmission model to study the direct radiation effect on terrestrial ecosystems from 2003 to 2010, and reported that enhanced R_d led to an increase of global GPP by 4.9 Pg C. Thus, previous studies clearly show that the impacts of R_d on the carbon cycle should be considered in ecological models.

In recent years, given the important influence of R_d on GPP, an increasing body of research has attempted to improve ecological models for simulation of GPP with the inclusion of R_d with LUE models. The two-leaf light use efficiency model (TL-LUE) simulates GPP with the differentiation of direct radiation and R_d [12]. Wang et al. [13,14] incorporated R_d into a LUE model. Yan et al. [15] also established a two-leaf model Terrestrial Ecosystem Carbon flux (DTEC) to separately simulate GPP for sunlit and shaded leaves. Zheng et al. [16] upgraded a large-leaf model, Eddy Covariance - Light Use Efficiency (EC-LUE), into a two-leaf model to separately simulate GPP for sunlit and shaded leaves. The above-mentioned models show that incorporation of R_d into GPP models clearly improves the GPP simulation.

In China, previous studies of changes in R_g and R_d have been based on meteorological data, including global radiation measurements, or global radiation derived from sunshine duration. With regard to R_g, studies of trends in R_g that were conducted around or before 2000 were inconsistent because of limited radiation measurement stations. Previous studies have shown that, during the period from the 1950s to 2000s, R_g changes in China have undergone a shift from darker (decreasing) to brighter (increasing) values [17–21], whereas other studies have shown that R_g in China has experienced a sustained reduction of about 3.1–4.5 W m^{-2} $decade^{-1}$ [22–24]. Studies on the trend of R_g based on an increased number of radiation measurement stations from the 1980s to the 2010s have shown that global radiation shows a distinct increasing trend [25]. Regarding R_d, previous studies have reported that, in the context of global dimming, R_d and the diffuse radiation fraction are increasing [19,22,25]. For example, Ren et al. [25] observed that national annual mean R_d during the period from 1981 to 2010 increased by 7.03 MJ m^{-2} y^{-1} by interpolation from 754 meteorological stations and 122 radiation stations across China. Che et al. [22] reported that the diffuse radiation fraction in China increased by 1.73% per decade from the 1960s to the 1990s.

Several studies have simulated the effects of changes in R_d and R_g on GPP at the site scale in China. He et al. [26] observed that increments in the diffuse radiation fraction enhanced the LUE of the forest canopy, which compensated for the reduction in GPP caused by the decrease in the PAR fraction in three forest ecosystems in China. Li et al. [27] reported that the response of canopy GPP to radiation changes was predominantly determined by the R_d in an evergreen coniferous forest in China. However, at a regional scale in China, the impacts of recent changes in R_g and R_d on GPP are unclear, which demands a better understanding and accurate spatiotemporal estimation of such impacts. The aims of the present study were to (i) analyze the trends of R_d and R_g in China from 1981 to 2012, and (ii) assess the effects of variation in the diffuse radiation fraction on terrestrial GPP in China.

2. Materials and Methods

2.1. Data

The data used in the two-leaf light use efficiency model (TL-LUE) model to simulate GPP in China over the period 1981–2012 were as follows: (i) grid-based meteorological data, including R_g, R_d, air temperature (T_a), minimum temperature (T_{amin}), maximum air temperature (T_{amax}), and vapor pressure deficit (VPD) at the daily scale; (ii) 8-day remotely sensed leaf area index (LAI); and (iii) remotely sensed land-cover data.

2.1.1. Meteorological Data

Average daily T_a, T_{amin}, T_{amax}, average relative humidity (RH), and sunshine duration for 1981–2012, available from 754 conventional meteorological stations, were used. The average RH was converted to VPD following the reference methodology of Allen et al. [28]. Of the 754 meteorological stations, R_g and R_d were measured at 103 and 81 sites, respectively, and sunshine duration was measured at all 754 sites during 1981–2012 (Figure 1 and Supplementary Figure S1, and Supplementary Tables S1 and S2).

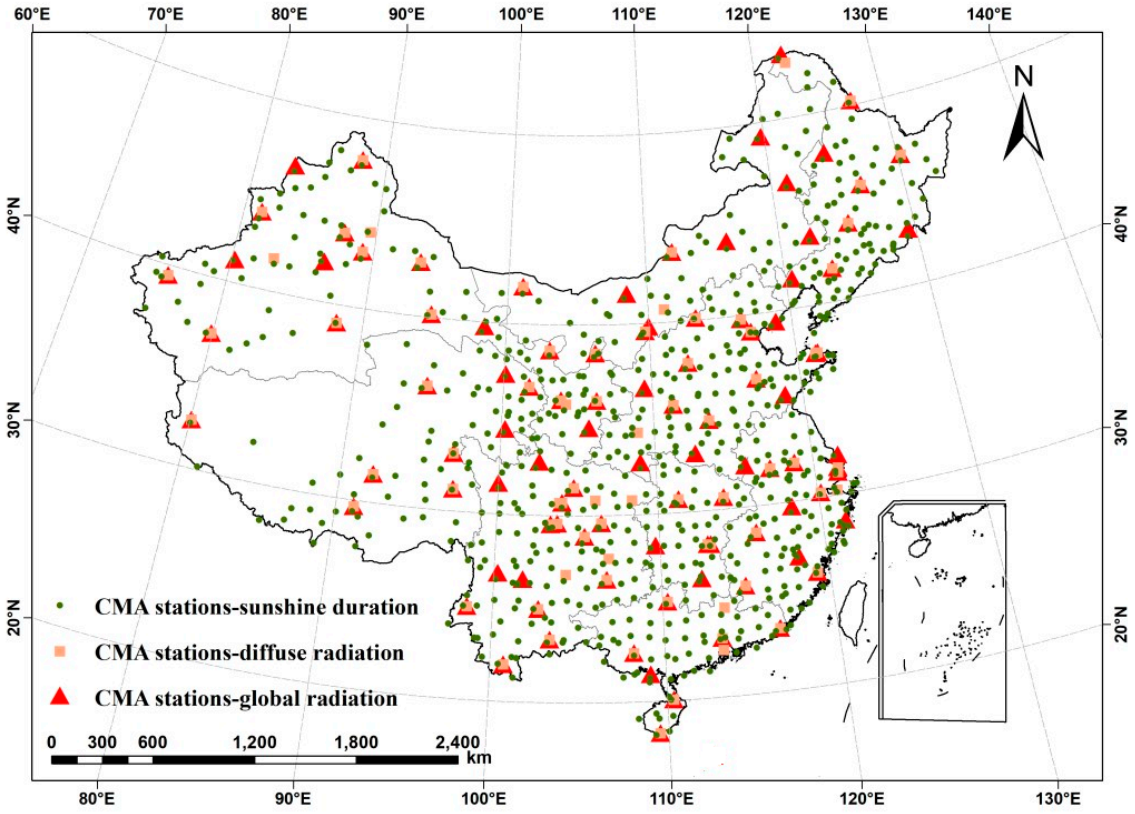

Figure 1. Distribution in China of meteorological stations recording sunshine duration, and global and diffuse radiation.

The R_g at the site scale was interpolated to the national scale by the following steps. First, the Ångström model (Equation (1)) [29] was calibrated using data from 103 meteorological stations recording both R_g and sunshine duration measurements during 1981–2012. Second, to compensate for the lack of global radiation measurements, R_g for the remaining 651 meteorological stations was calculated by using sunshine duration and the calibrated Ångström model in step 1. Third, data from 12 sites with R_g measurements in 2014 were used to validate the calibrated Ångström model (see

Supplementary Materials Figure S2). Finally, using radiation data at the 754 sites, R_g was interpolated to the national scale with an inverse distance weighted method.

Considering the heterogeneity of terrain and climate in China, the country was divided into eight regions: Northeast China (R1), Inner Mongolia (R2), Northwest China (R3), North China (R4), Central China (R5), South China (R6), Southwest China (R7), and the Qinghai–Tibet Plateau (R8). The R_g estimation model was fitted for each region separately to convert sunshine duration into R_g, which was comparable with the method of Ren et al. [25,30]. The Ångström model [29] was selected to estimate R_g because of the advantages of a simple structure, clear physical meaning, stable model coefficients, and good fitting results in addition to its widespread use [31]. This model was as follows:

$$\frac{R_g}{R_0} = a + b \times \frac{n}{N} \quad (1)$$

where R_g is the global radiation reaching the surface, R_0 is the daily extraterrestrial radiation, n is the actual daily sunshine duration observed at a given site, N is the potential daily sunshine duration, and a and b are coefficients. Both R_0 and N can be calculated based on latitude and date [32]. Root mean square error (RMSE) values of the radiation derived using Ångström models for each of the eight regions of China are shown in Table 1.

Table 1. Parameter and error values for the various Ångström models used to convert sunshine hours into global radiation (R_g) for eight regions of China.

Parameters	R_1	R_2	R_3	R_4	R_5	R_6	R_7	R_8
a	0.234	0.234	0.214	0.213	0.226	0.238	0.230	0.232
b	0.501	0.505	0.527	0.479	0.450	0.457	0.498	0.556
Samples	78.503	86.281	195.870	165.151	166.877	54.146	62.710	124.354
R^2	0.714	0.665	0.726	0.733	0.739	0.749	0.788	0.687
Root Mean Square Error (RMSE, MJ m^{-2} d^{-1})	2.180	2.219	2.073	2.130	2.394	2.378	2.442	3.056

The R_d at the site scale was interpolated to the national scale based on the following steps. First, data from 81 meteorological stations recording both R_g and R_d during 1981–2012 were used to calibrate the logistic model (Equation (2)) [27,30]. Second, to compensate for the lack of R_d measurements, R_g estimated with the Ångström model was used to calculate R_d for the remaining 673 meteorological stations using the calibrated Equation (2) in step 1. Third, data from 12 sites with R_g measurements in 2014 were used to validate the calibrated Ångström model (see Supplementary Materials, Figure S3). Finally, R_d was interpolated to the national scale using R_d at the 754 sites.

A simple and accurate logistic model [27,30] was used to estimate R_d as follows:

$$\frac{R_d}{R_g} = \frac{1}{1 + e^{c + d \times \frac{R_g}{R_0}}} \quad (2)$$

where R_d is the diffuse radiation, and c and d are the nonlinear regression coefficients. Table 2 shows the RMSE values of estimated R_d derived from logistic models for the eight regions of China.

Table 2. Parameters and error values for various logistic models used to estimate diffuse radiation (R_d) for eight regions of China.

Parameters	R_1	R_2	R_3	R_4	R_5	R_6	R_7	R_8
c	−2.936	−3.454	−3.760	−3.976	−3.759	−3.418	−3.513	−2.850
d	5.657	6.161	6.778	7.338	7.054	6.647	6.796	5.741
Samples	26.788	11.483	79.589	46.943	59.732	15.704	19.647	37.161
R^2	0.695	0.712	0.707	0.811	0.779	0.696	0.797	0.630
RMSE (MJ m^{-2} d^{-1})	1.727	1.955	2.115	1.596	1.715	2.254	1.821	2.516

The coefficient of determination (R^2) for R_g and R_d measurements and estimations ranged from 0.66 to 0.79 (Table 1) and 0.63 to 0.81 (Table 2), which were comparable with the results of Singh [33] and Ren et al. [30]. Validation (see Supplementary Materials, Figures S2 and S3) indicated that the R^2 for R_g measurements and estimations was 0.85–0.96 and that for R_d was 0.55–0.75 at validation sites. Estimated global and R_d in this study showed the similar values to those of Ren et al. [30] (see Supplementary Materials, Figure S4).

2.1.2. LAI Data

The LAI at a 0.0727° grid for 1981–2012 was generated using the Moderate Resolution Imaging Spectroradiometer (MODIS) and the Advanced Very High Resolution Radiometer (AVHRR) data. The dataset was generated by Liu et al. [34] and has been widely used in studies of the carbon cycle and vegetation response to climate change of terrestrial ecosystems [35–39]. GLOBMAP LAI V3 during 1981 to 2012 was generated by fusing LAI inverted from MODIS reflectance data with Global Inventory Modelling and Mapping Studies (GIMMS) AVHRR Normalized Difference Vegetation Index (NDVI) data. The LAI from 2001 to 2012 was first derived from the MODIS land surface reflectance data (MOD09A1) reflectance based on the GLOBCARBON LAI algorithm. For the fusion of MODIS and AVHRR remotely sensed data, the relationships between GIMMS NDVI and MODIS LAI were established pixel by pixel over a period (2001–2006) that they overlap. The AVHRR LAI from 1981 to 2000 was then generated using these relationships.

2.1.3. Land-cover Data

Given the lack of land-cover data before 2000, we used land-cover data in 2001 for the entire period simulations. The MODIS land-cover data at 500-m spatial resolution (MCD12Q1) for 2001 was resampled to 0.0727° to drive the TL-LUE model during 1981 and 2012. The International Geosphere–Biosphere Programme classification system was used in this study, including categories of evergreen needle-leaf forest (ENF), deciduous coniferous forest (DNF), evergreen broad-leaved forest (EBF), deciduous broad-leaved forest (DBF), evergreen broad-leaved forest (ENF), deciduous coniferous forest (DNF), evergreen broad-leaved forest (EBF), mixed forest (MF), sparse shrubland (OS), dense shrubland (CS), grassland (GRASS), farmland (CROP), and other surface cover types (NOV).

2.1.4. GPP Data

Flux data from 13 available flux tower sites of the ChinaFLUX network were compared with the simulated GPP. These sites included three broad-leaved forest (BF), two needle-leaved forest (NF), one MF, one shrubland (Shrub), four GRASS, and two CROP sites, providing a total of 100 site years (Table 3).

Table 3. Specifications for the 13 flux tower sites. (BF means broad-leaved forest; CROP means crop; GRASS means grass; MF means mixed forest; NF means needle-leaved forest; Shrub means shrubland).

Name	Latitude (°)	Longitude (°)	Years	Vegetation Types
Xishuangbanna (XSBN)	21.95	101.2	2003–2012	BF
Dinghushan (DHS)	23.17	112.53	2003–2011	BF
Ailaoshan (ALS)	24.54	101.03	2009–2011	BF
Luancheng (LC)	37.88	114.68	2009–2012	CROP
Yucheng (YC)	36.83	116.57	2003–2012	CROP
Haibei2 (HB)	37.61	101.33	2003–2012	GRASS
Neimeng (NM)	43.53	116.67	2004–2012	GRASS
Duolun (DL)	42.03	116.28	2010–2012	GRASS
Dangxiong (DX)	30.5	91.07	2004–2011	GRASS
Changbaishan (CBS)	42.4	128.1	2003–2011	MF
Qianyanzhou (QYZ)	26.73	115.07	2003–2012	NF
Huitong (HT)	26.79	109.59	2008–2012	NF
Haibei1 (HBG)	37.67	101.33	2003–2012	Shrub

2.2. Modeling

2.2.1. TL-LUE Model

The TL-LUE model [12] is based on MODIS GPP [40] and the Boreal Ecosystem Productivity Simulator (BEPS) model [41]. Model validation was performed at both the site [42,43] and the regional scale [44]. Additional information on the model was introduced in [12,42,43]. The model parameters used for the TL-LUE models followed Zhou et al. [43].

GPP was calculated with the following Equation (3):

$$\mathrm{GPP} = (\varepsilon_{\mathrm{msu}} \times \mathrm{APAR}_{\mathrm{su}} + \varepsilon_{\mathrm{msh}} \times \mathrm{APAR}_{\mathrm{sh}}) \times f(\mathrm{VPD}) \times f(T_{\mathrm{amin}}) \quad (3)$$

where $\varepsilon_{\mathrm{msu}}$ and $\varepsilon_{\mathrm{msh}}$ are the maximum LUE of sunlit and shaded leaves, respectively; $\mathrm{APAR}_{\mathrm{su}}$ and $\mathrm{APAR}_{\mathrm{sh}}$ are the absorbed PAR of sunlit and shaded leaves, respectively; and $f(\mathrm{VPD})$ and $f(T_{\mathrm{amin}})$ are stress factors of Vapour Pressure Deficiency (VPD) and air temperature, respectively. $\mathrm{APAR}_{\mathrm{su}}$ and $\mathrm{APAR}_{\mathrm{sh}}$ were calculated with the following Equations (4) and (5):

$$\mathrm{APAR}_{\mathrm{su}} = (1-\alpha) \times [\mathrm{PAR}_{\mathrm{dir}} \times \cos(\beta)/\cos(\theta) + (\mathrm{PAR}_{\mathrm{dif}} - \mathrm{PAR}_{\mathrm{dif,u}})/\mathrm{LAI} + C] \times \mathrm{LAI}_{\mathrm{su}} \quad (4)$$

$$\mathrm{APAR}_{\mathrm{sh}} = (1-\alpha) \times [(\mathrm{PAR}_{\mathrm{dif}} - \mathrm{PAR}_{\mathrm{dif,\,u}})/\mathrm{LAI} + C] \times \mathrm{LAI}_{\mathrm{sh}} \quad (5)$$

where α is albedo; $\mathrm{PAR}_{\mathrm{dif\_u}}$ is diffuse radiation under the canopy; C is multiple scattered radiation; β is the leaf angle, which was considered to be 60°; θ is the solar zenith angle; $\mathrm{PAR}_{\mathrm{dif}}$ and $\mathrm{PAR}_{\mathrm{dir}}$ are incoming direct and diffuse radiation, respectively (Chen et al., 1999). $\mathrm{LAI}_{\mathrm{su}}$ and LAIsh are the LAI of sunlit and shaded leaves and was calculated with Equations (6) and (7):

$$\mathrm{LAI}_{\mathrm{su}} = 2 \times \cos(\theta) \times (1 - \exp(-0.5\mathrm{LAI}/\cos(\theta))) \quad (6)$$

$$\mathrm{LAI}_{\mathrm{sh}} = \mathrm{LAI} - \mathrm{LAI}_{\mathrm{su}} \quad (7)$$

On the basis of Equations (3)–(5), GPP derived from diffuse radiation can be calculated with the following Equation (8):

$$\mathrm{GPP}_{\mathrm{dif}} = \left(\varepsilon_{\mathrm{msu}} \times \left((1-\alpha) \times \frac{\mathrm{PAR}_{\mathrm{dif}} - \mathrm{PAR}_{\mathrm{dif,u}}}{\mathrm{LAI}}\right) \times \mathrm{LAI}_{\mathrm{msu}} + \varepsilon_{\mathrm{msh}} \times \left((1-\alpha) \times \frac{\mathrm{PAR}_{\mathrm{dif}} - \mathrm{PAR}_{\mathrm{dif,u}}}{\mathrm{LAI}}\right) \times \mathrm{LAI}_{\mathrm{msh}}\right) \times f(\mathrm{VPD}) \times g(T\mathrm{a\ min}) \quad (8)$$

where $\mathrm{GPP}_{\mathrm{dif}}$ and $\mathrm{GPP}_{\mathrm{dir}}$ are GPP contributed by diffuse and direct radiation, respectively.

2.2.2. Modeling Scenarios

To quantitatively assess the impacts of variation in R_g and diffuse radiation fractions on GPP, three simulations were performed (see Supplementary Materials, Table S3).

(i) Scenario 1 (Scenario): Both historical meteorological data with temporal variations and LAI were used to simulate GPP for the period 1981–2012.

(ii) Scenario 2 (Scenario_R_g): Temporally constant R_g data, other historical meteorological data with temporal variations, and LAI were used to simulate GPP for the period 1981–2012. The differences between simulated GPP values in S1 and S2 reflect the effects of change in R_g on GPP simulation.

Based on the assumption that the annual R_g remained unchanged from 1981 to 2012, and the variation tendency of daily R_g variation to R_g averaged values during 1981–2012 was consistent, daily radiation for the period 1982–2012 was calibrated using Equation (9):

$$R^k_{(i,j)|m} = \frac{\sum_{k=1}^{365} R^k_{(i,j)|year=1981}}{\sum_{k=1}^{365} R^k_{(i,j)|year=m}} \times R^k_{(i,j)|m} \quad m = 1981, 1982, \ldots, 2012; k = 1, 2, \ldots, 365 \tag{9}$$

where i and j are the line and row of any given pixel, and $R^k_{(i,j)|m}$ is the daily R_g of pixel (i, j) on the kth day of the mth year.

(iii) Scenario 3 (Scenario_R_d): Temporally constant R_d, other historical meteorological data with temporal variations, and LAI were used to simulate GPP for the period 1981–2012. The difference between simulated GPP values in S1 and S3 reflect the effects of R_d on GPP simulations.

Based on the assumption that the annual diffuse radiation fraction remained constant from 1981 to 2012, and the variation tendency of daily R_d variation to R_d averaged values during 1981–2012 was consistent, the daily diffuse radiation fraction for the period 1982–2012 was calibrated using Equation (10):

$$f^k_{dif(i,j)|m} = \frac{\sum_{k=1}^{365} f^k_{dif(i,j)|year=1981}}{\sum_{k=1}^{365} f^k_{dif(i,j)|year=m}} \times f^k_{dif(i,j)|m} \quad m = 1981, 1982, \ldots, 2012; k = 1, 2, \ldots, 365 \tag{10}$$

where i and j are the row and column of a given pixel, and $f^k_{dif(i,j)|m}$ is the diffuse radiation fraction in pixel (i, j) for the kth day of the mth year. The diffuse radiation fraction was calculated using Equation (11):

$$f_{\mathrm{dif}} = R_d/R_g \tag{11}$$

where f_{dif} is the diffuse radiation fraction, R_d and R_g are diffuse and global radiation, respectively.

3. Results

3.1. Spatiotemporal Distributions of Annual Radiation in China

The spatial distributions of the average annual and standard deviation of R_g, R_d, and diffuse radiation fraction in China over the period 1981–2012 are shown in Figure 2. The R_g (Figure 2a) was unevenly distributed across China, with a range of 3255–7154 MJ m^{-2} y^{-1} and a national average of 5258 MJ m^{-2} y^{-1} (Figure 2a). The standard deviation of R_g ranged from 65 to 359 MJ m^{-2} y^{-1} (Figure 2b). Generally, R_g values on the western plateau were higher than those on the eastern plain. The highest R_g values were recorded on the southern part of the Qinghai–Tibet Plateau (>6500 MJ m^{-2} y^{-1}) because of the thin air density in this region. The northeastern part of the Sichuan Basin and the Yunnan–Guizhou Plateau had the lowest annual R_g values (<3800 MJ m^{-2} y^{-1}).

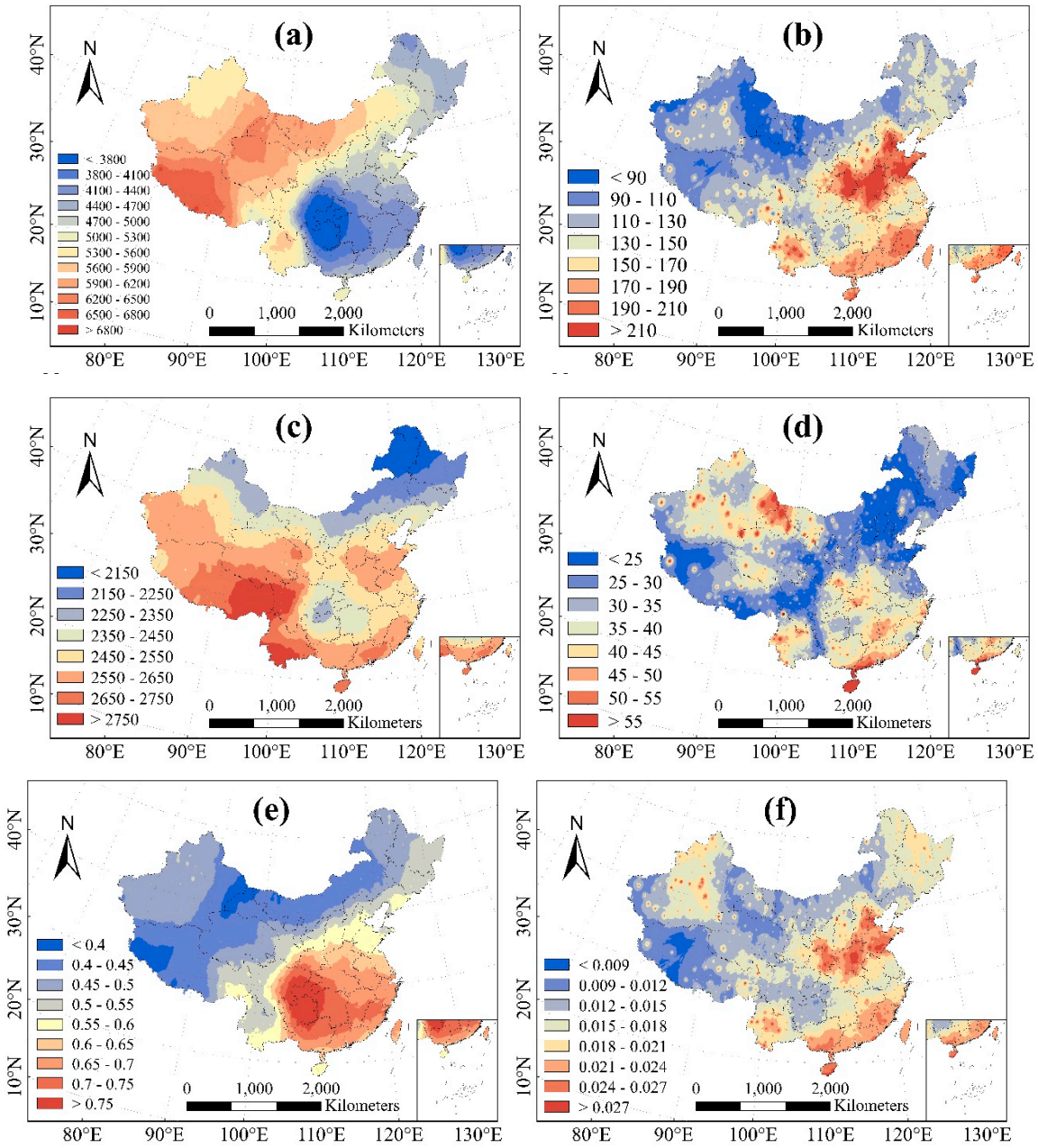

Figure 2. Spatial distribution of the mean (**a**) and standard deviation (**b**) of global radiation (unit: MJ m^{-2} y^{-1}), the annual mean (**c**) and standard deviation (**d**) of diffuse radiation (unit: MJ m^{-2} y^{-1}), and the mean (**e**) and standard deviation (**f**) of diffuse radiation fraction in China for the period 1981–2012 with a spatial resolution of 0.0727°.

Values of R_d (Figure 2c) ranged from 1989 to 3007 MJ m^{-2} y^{-1} and showed a national average of 2483 MJ m^{-2} y^{-1}, which is close to the value of 2477 MJ m^{-2} y^{-1} estimated by Ren et al. [25,30]. The standard deviation range of R_g is 15–101 MJ m^{-2} y^{-1} with a national average of 33 MJ m^{-2} y^{-1} (Figure 2d). In general, R_d was high in the south and west of China and low in the north. The highest values of R_d were on the Qinghai–Tibet Plateau and on the southwestern part of the Yunnan–Guizhou Plateau, with values higher than 2800 MJ m^{-2} y^{-1}. The lowest values were found for Northeast China, Inner Mongolia, and Northwest China, with values of less than 2300 MJ m^{-2} y^{-1}. Values of diffuse radiation fraction ranged from 0.34 to 0.83 and showed a national average of 0.52 (Figure 2e), and the diffuse radiation fraction was highest in southern China, especially within the regions of Sichuan

and Guizhou. The standard deviation of diffuse radiation fraction ranged from 0.007 to 0.043 with a national average of 0.016 (Figure 2f).

The R_g exhibited broad variability during 1981–2012 but generally showed a significant ($p < 0.05$) negative trend of 2.18 MJ m^{-2} y^{-1}, yielding a rate of decrease of 1.3% y^{-1} (Figure 3a). Specifically, R_g decreased markedly and then increased slightly during the interval 1980–1990. During the interval 1991–1993, R_g declined rapidly, possibly because of the volcanic eruption of Mount Pinatubo in 1991. This volcanic eruption led to the release of about 20 million tonnes of sulfide gas into the stratosphere, producing a reduction in R_g. The R_g values were gradually restored after 1994 [9,25,30]. Values of R_g also decreased slightly after 1999, consistent with the findings of Che et al. [22] and Wild et al. [17].

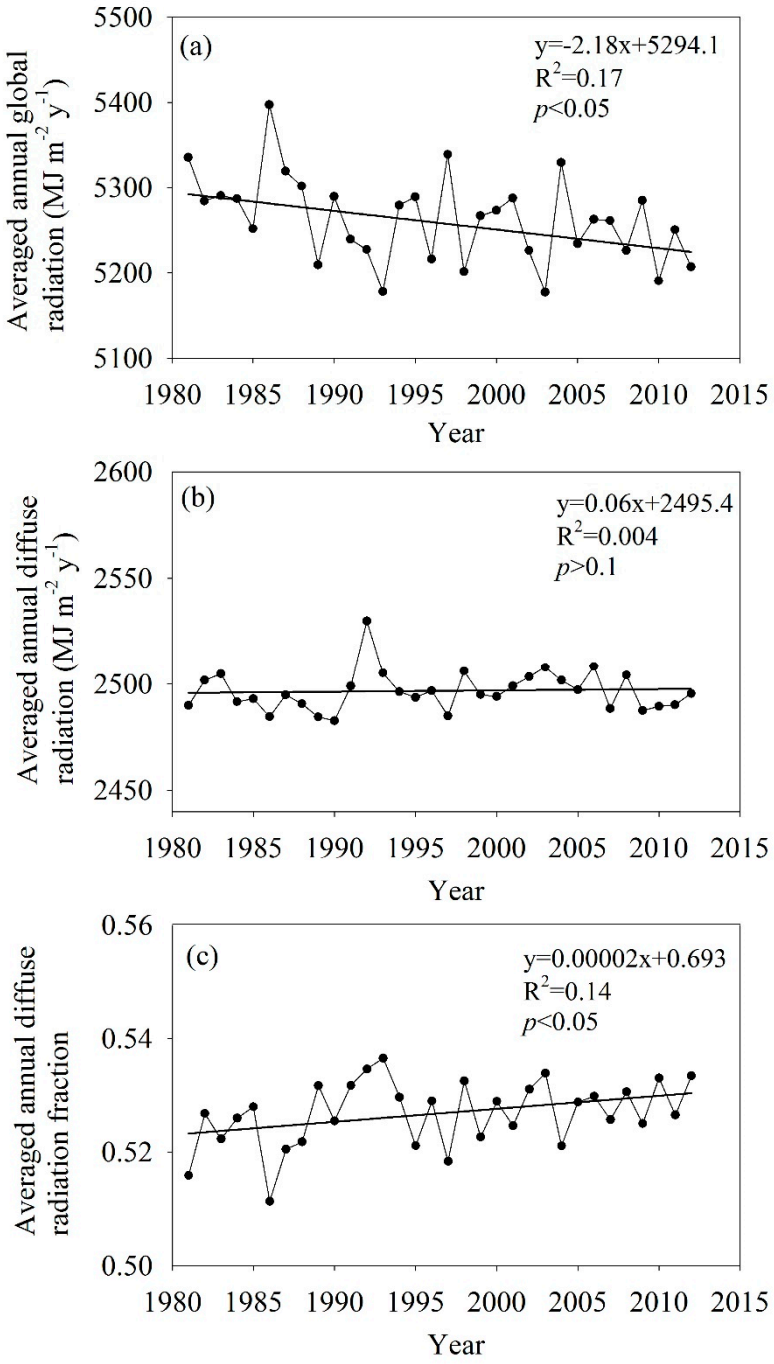

Figure 3. Linear trends in annual mean (**a**) global radiation, (**b**) diffuse radiation, and (**c**) diffuse radiation fraction across China for the period 1981–2012.

The simple linear trend in the average annual R_d in China was positive from 1981 to 2012, although this trend was not significant (Figure 3b). The R_d decreased during the interval 1981–1990 but increased and then decreased rapidly during the interval 1991–1994 because of the eruption of Mount Pinatubo. From the mid-1990s, R_d increased slightly and then decreased again.

The annual average diffuse radiation fraction in China increased markedly between 1981 and 2012 by 0.0002 y^{-1} ($p < 0.05$) (Figure 3c).

The spatial distribution of the variation in annual R_g, R_d, and diffuse radiation fraction in China over the period 1981–2012 is shown in Figure 4. Decreases in R_g mainly occurred in North China, Hainan, and on the Qinghai–Tibet Plateau (Figure 4a), which is consistent with the findings of Tang et al. [45] and Lin et al. [46]. Conversely, R_g increased only over a small part of China during the period 1981–2012. Generally, the changes in R_g over most parts of China were not significant, predominantly because China experienced "dimming" prior to 1990, whereas R_g increased slightly over large parts of China post-1990 [23].

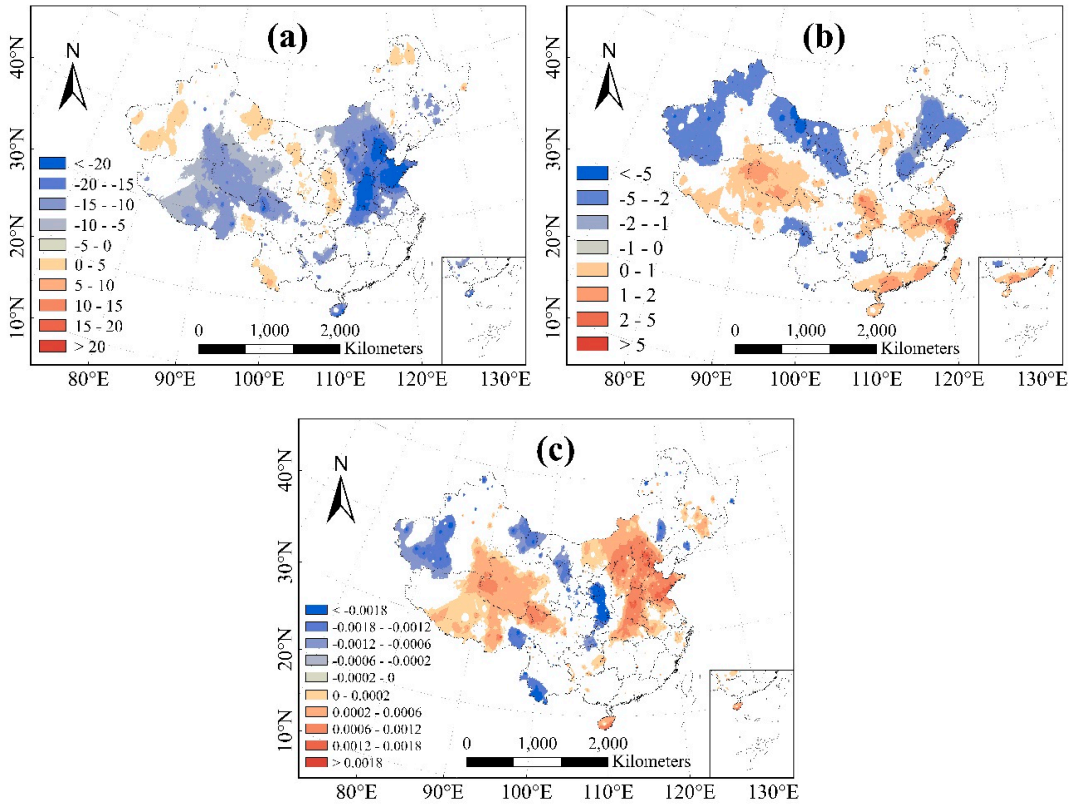

Figure 4. Spatial distribution of the changing rate in annual mean global radiation ((**a**), unit: MJ m^{-2} y^{-1}), diffuse radiation ((**b**), unit: MJ m^{-2} y^{-1}), and diffuse radiation fraction (**c**) in China for the period 1981–2012 (white areas show no significant trends; $\alpha = 0.05$) with a spatial resolution of 0.0727°.

Increases in R_d predominantly occurred over the Qinghai–Tibet Plateau, Shanghai–Hangzhou–Wuhan region, Guangdong, and Guangxi and its surrounding areas (Figure 4b). Decreases in R_d occurred in the northwestern part of Xinjiang, western parts of Inner Mongolia, and Shenyang. The national average diffuse radiation fraction increased by 0.2% $decade^{-1}$ during the period 1981–2012 (Figure 4c). Initially, the diffuse radiation fraction increased and then decreased during the 1980s. In 1993, after the eruption of Mount Pinatubo, the diffuse radiation fraction attained its peak during the study period, and then quickly returned to its average value.

3.2. Spatial Distribution of GPP in China over the Period 1981–2012

At the site scale, comparison of the simulated GPP values derived from the TL-LUE model (GPPTL) versus site flux data-derived GPP showed good agreement (R^2 = 0.82; N = 100; $p < 0.0001$) (Figure 5). At the national scale, the average annual GPP value in China was estimated to be 7.64 Pg C y^{-1}, which lies within the range of values reported by previous studies (Table 4). Li et al. [47] estimated the average annual GPP from 2001 to 2010 as 6.04 Pg C y^{-1}, and the annual mean GPP value based on MODIS for China for the same period was estimated as 5.47 Pg C y^{-1}. The GPP estimates based on relationships with meteorological data were 6.06 and 7.78 Pg C y^{-1} during 2001–2010 with two spatial resolutions [48].

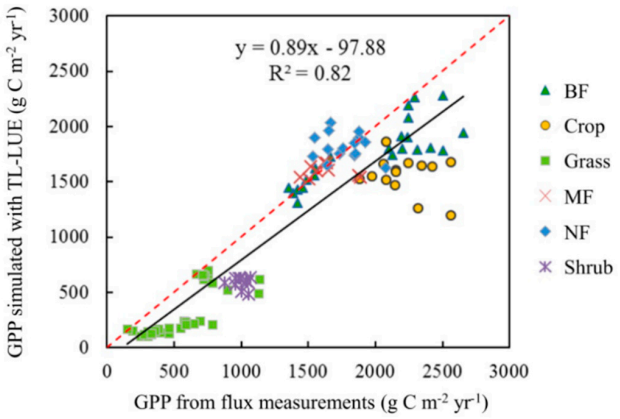

Figure 5. GPP derived from observations at each of 13 flux tower sites and the GPP values estimated by the TL-LUE model. BF, broad-leaved forest; MF, mixed forest; NF, needle-leaf forest.

The multi-year mean GPP in China for the period 1981–2012 is shown in Fig. 6a. In the southeastern and northeastern parts of China, the GPP was higher than 1000 g C m^{-2} y^{-1}. On the southeastern coast, Yunnan–Guizhou Plateau, and the southern part of the Qinghai–Tibet Plateau, the GPP was higher than 2500 g C m^{-2} y^{-1}. Low values of GPP occurred over desert areas of China and the remaining parts of the Qinghai–Tibet Plateau. Given the scarcity of vegetation in these areas, their annual GPP values were less than 50 g C m^{-2} y^{-1}. The northern Tianshan Mountains showed high GPP values of up to 1000–2000 g C m^{-2} y^{-1}. Inner Mongolia and the southeastern part of the Qinghai–Tibet Plateau formed part of a transition zone to lower values, showing annual GPP values of 200–1000 g C m^{-2} y^{-1}. Therefore, the TL-LUE model's simulation of the average annual distribution of GPP was reasonable and was largely consistent with previous simulations [44,47]. The standard deviation of GPP during 1981–2012 showed a national average of 75 g C m^{-2} y^{-1} with a range of 0–838 g C m^{-2} y^{-1} (Figure 6b).

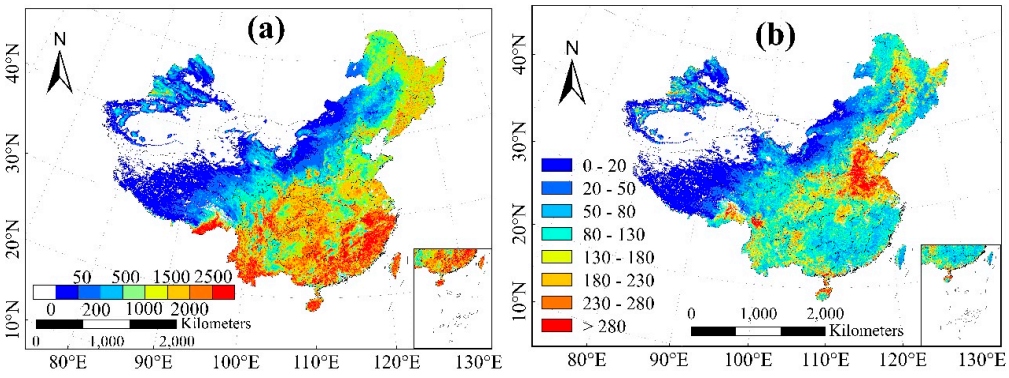

Figure 6. Spatial distribution of the annual GPP (**a**) and standard deviation of GPP (**b**) estimated by the TL-LUE model for the period 1981–2012 (unit: g C m^{-2} y^{-1}) with a spatial resolution of 0.0727°.

Table 4. Comparison between gross primary productivity (GPP) of major vegetation types and total annual GPP estimated using TL-LUE and other models (ENF means evergreen needle-leaved forest; EBF means evergreen broad-leaved forest; DNF means deciduous needle-leaved forest; DBF means deciduous broad-leaved forest).

Model Types	Model	ENF	EBF	DNF	DBF	MF	Shrub	GRASS	CROP	Time	Resolution	Annual Total GPP	References
LUE model	TL-LUE	1.210 (±49)	1.720 (±32)	798 (±52)	1.090 (±32)	1.620 (±46)	625 (±42)	210 (±24)	1.308 (±72)	1981–2012	0.0727°	7.64 (±0.33)	This study
	TL-LUE									2007–2011	0.0727°	7.17	[44]
	MODIS									2001–2010	10 km	5.47	[47]
	EC-LUE	992	1.430	829	1.083	1.273	244–775	382	948 [a]	2001–2010	10 km	6.04	[47]
	GLOPEM	710 [a]	1.436 [a]	734 [a]	902 [a]	1.338 [a]	1.232 [a]	290 [a]	744 [a]	1981–2000	8 km	5.52–6.62 [a]	[49]
	GEOLUE	1.172 [a]	2.172 [a]	1.314 [a]	1.130 [a]	1.914 [a]	1.446 [a]	356 [a]	724 [a]	2000–2004	8 km	5.68 [a]	[49]
	CASA	928 [a]	1.122 [a]	996 [a]	1.030 [a]	1.092 [a]	984 [a]	490 [a]	730 [a]	1982–2003	8 km	5.14–5.92 [a]	[49]
	CASA	491 [a]	836 [a]	569 [a]	490 [a]	592 [a]	516 [a]	289 [a]	853 [a]	1982–1999	0.1°	2.66–3.16 [a]	[50]
	CASA	734 [a]	1.972 [a]	878 [a]	1.286 [a]		735 [a]	207–1015 [a]	1.782 [a]	1989–1993	8 km	6.24 [a]	[51]
Process model	BEPS	938 [a]	1.480 [a]	844 [a]	998 [a]	1.119 [a]	726 [a]	245 [a]	872 [a]	2001	1 km	4.418 [a]	[52]
	TEM					1.246 [a]	168 [a]	384–470 [a]		1993–1996	0.5°	7.31 [a]	[53]
	CEVSA	716 [a]	1.436 [a]	704 [a]	944 [a]	1.414 [a]	1.400 [a]	416 [a]	1.154 [a]	1981–1998	0.5°	6.18 [a]	[54]
	CEVSA	972 [a]	1.746 [a]	690 [a]	1.248 [a]	846 [a]	982 [a]	696 [a]	1.212 [a]	1980–2000	10 km	6.26–7.36 [a]	[49]
	GEOPRO	498 [a]	1.244 [a]	536 [a]	632 [a]	1.250 [a]	1.122 [a]	336 [a]	688 [a]	2000	4 km	4.84 [a]	[49]
Others	Geographical assessment									2001–2010	1 km	7.78 [a]	[48]
	Model tree ensemble									2001–2010	0.5°	6.06 [a]	[48]

Note: The units for mean GPP and national total GPP are g C m^{-2} y^{-1} and Pg C y^{-1}, respectively. [a] Only data for net primary productivity (NPP) were reported (NPP/GPP = 0.5)

3.3. Spatial Distribution of Diffuse Radiation Contribution to Terrestrial Ecosystem GPP

The spatial distribution of GPP driven by R_d was consistent with that of GPP driven by R_g (Figure 7a–b). GPP driven by Rd ranged from 0 to 4348 g C m^{-2} y^{-1} with a national average of 586 g C m^{-2} y^{-1} and a national average standard deviation of 56 g C m^{-2} y^{-1}. Figure 7c,d show the proportion of GPP fixed by R_d to the total GPP and its standard deviation. The proportion of GPP fixed by R_d to the total GPP ranged from 0.43 to 0.88 with a national average of 0.71, with very low standard deviation ranging from 0.0007 to 0.12. The highest proportion was in the northern Sichuan Basin and the northern parts of the Yunnan–Guizhou Plateau, where the diffuse radiation fraction was highest. Conversely, in most parts of northwestern and northeastern China, the diffuse radiation fraction was less than 0.5 (Figure 2e), where the proportion of GPP contributed by R_d to GPP derived from R_g was greater than 0.5, reflecting the higher LUE of R_d.

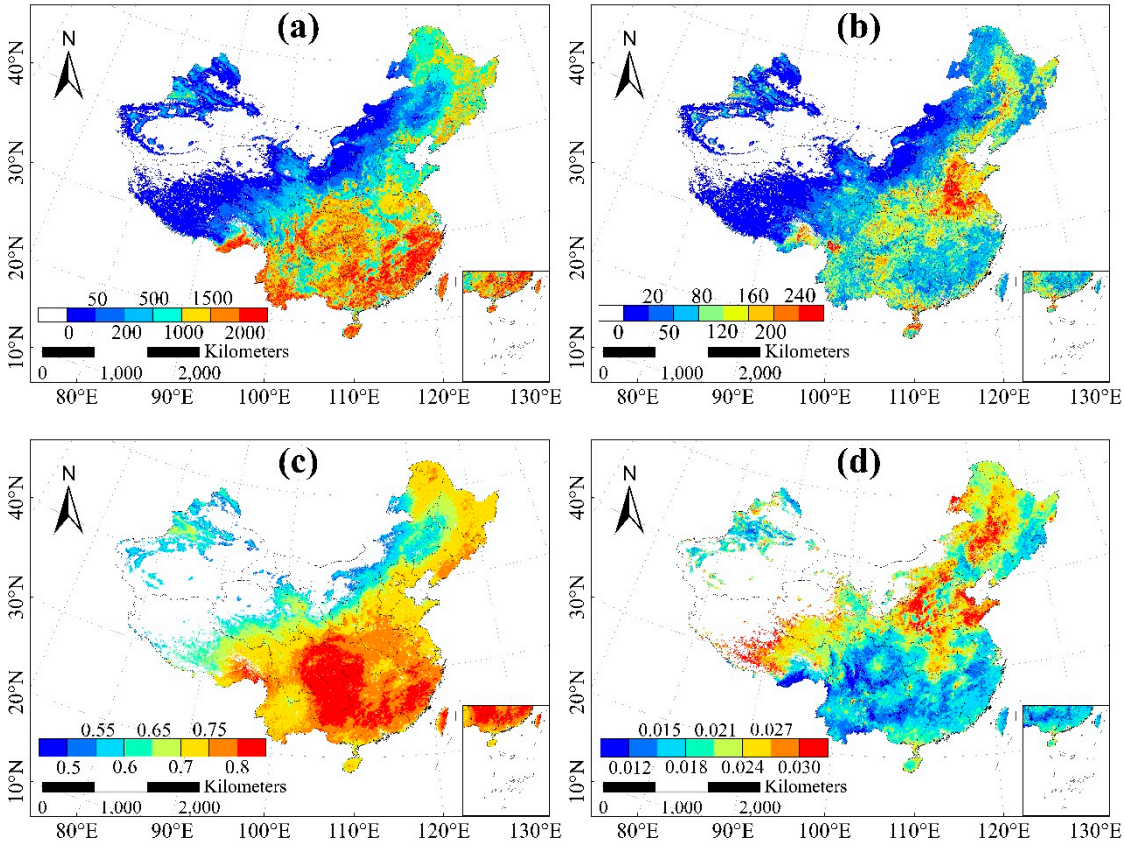

Figure 7. Spatial distribution of the annual (**a**) GPP sequestrated by diffuse radiation (unit: g C m^{-2} y^{-1}) and its standard deviation (**b**), and the ratio of annual mean (**c**) GPP sequestrated by diffuse radiation and global radiation and its standard deviation (**d**) during the period 1981–2012 with a spatial resolution of 0.0727°.

3.4. Impact of Radiation Changes on GPP

3.4.1. Simulated Interannual Variability of Total GPP in China

The total amounts of GPP for China during the period 1981–2012 from three simulations are shown in Figure 8. In S1, the mean annual total GPP for the period 1981–2012 ranged from 7.43 to 8.47 Pg C y^{-1}. The total amount of GPP was lowest in 2000, likely because of the large-scale severe drought in China at that time. In S2, the multi-year mean annual GPP for the period 1981–2012 was 7.73 Pg C y^{-1}, which was 0.09 Pg C y^{-1} higher than the average value for S1. The difference in GPP between S1 and S2 reflects the effects of the 1.3% reduction in R_g, which caused a reduction of 1.7%

in GPP. In S3, the multi-year mean national total GPP was 7.58 Pg C y^{-1} for the period 1981–2012, which was higher than the average value for S1. The difference in GPP between S1 and S3 reflects the increase in the diffuse radiation fraction over the period 1981–2012, which positively affected GPP in China and partially compensated for the loss in GPP because of the reduction in R_g.

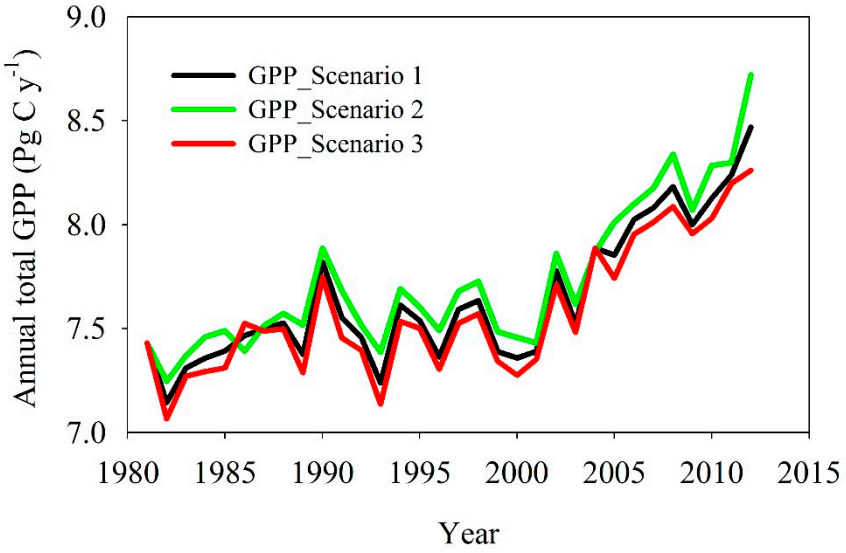

Figure 8. Interannual variation in total annual GPP for the period 1981–2012 in China for three simulations (GPP_Scenario 1; GPP_Scenario 2; and GPPsi GPP_Scenario 3). Scenario 1 assumed that the global radiation and diffuse radiation ratio changed with time; Scenario 2 assumed that global radiation remained unchanged from 1981 to 2012; and Scenario 3 assumed that the diffuse radiation fraction remained unchanged from 1981 to 2012.

3.4.2. Spatial Distribution of Radiation Effects on GPP

The average GPP in the period 1981–2012 simulated in S2 (Figure 9a) and S3 (Figure 9c) were similar to the distribution for S1 (Figure 6). The difference (Figure 9b) between the multi-year mean GPP simulated in S1 and S2 showed that any reduction in R_g would result in a reduction in GPP over most of China. In North China, the decrease in R_g was significant, simultaneously reducing the GPP by more than 50 g C m^{-2} y^{-1}. The R_g over Central and Southwest China showed no significant decrease, but these areas experienced a decrease in GPP that was higher than 50 g C m^{-2} y^{-1}, which was predominantly because of the high LAI in these regions (see Supplementary Materials, Figure S5). Compared with areas with lower LAI, the reduction in R_g substantially reduced GPP for regions with higher LAI. During the period 1981–2012, the areas that showed the highest GPP increase were along the southeastern coast, northern Sichuan, as well as northeastern, northern, and some western parts of Xinjiang.

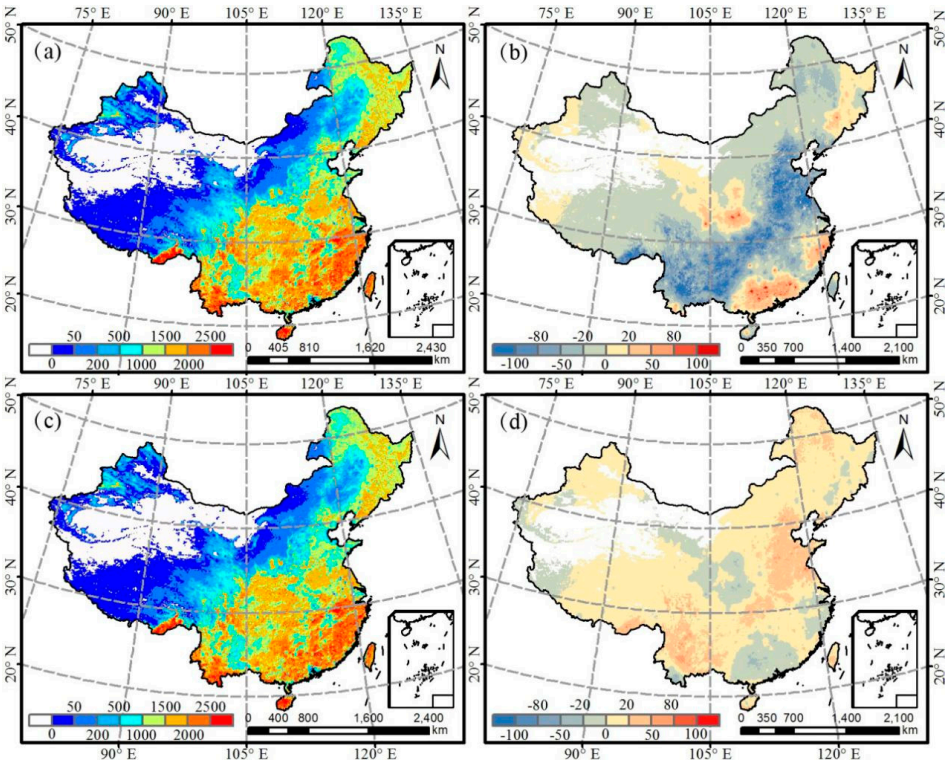

Figure 9. Spatial distribution of the mean annual GPP simulated by scenario 2 (**a**); spatial distribution of the difference between the mean annual GPP in simulations 1 and 2 (**b**); spatial distribution of the annual mean GPP in simulation 3 (**c**); and spatial distribution of the difference between the mean annual GPP in simulations 1 and 3 (**d**) (unit: g C m^{-2} y^{-1}). Simulation 1 assumed that the global radiation and diffuse radiation ratio changed with time; simulation 2 assumed that global radiation remained unchanged from 1981 to 2012; and simulation 3 assumed that the diffuse radiation fraction remained unchanged from 1981 to 2012 with a spatial resolution of 0.0727°.

The difference in GPP values between S1 and S3 are shown in Figure 9d. In most regions of China, the enhanced diffuse radiation fraction led to an increase in GPP, especially in Central China and Yunnan Province. The significant increase in GPP in Central China mainly resulted from the increase in R_d. In Yunnan Province, although the increase in diffuse radiation fraction was not significant, the GPP increased because of the high LAI (see Supplementary Materials, Figure S5). On the Qinghai–Tibet Plateau, although the diffuse radiation fraction significantly increased, the increase in GPP was not as strongly significant as that in Central China because of the scarcity of vegetation in the former region. Similarly, along the southeastern coast, in Xi'an and western parts of Xinjiang, the reduction in diffuse radiation fraction led to a reduction in GPP.

4. Discussion

In China, annual mean R_d has increased during the past 30 years [25]. An increase in R_d leads to an increase in canopy LUE because photosynthetic saturation is reduced, thereby enhancing the ecosystem GPP [3,5]. Therefore, investigating the effect of R_d on GPP is important in studies of the carbon cycle [5,8,9]. There are many causes of radiation changes, such as changes in the solar constant, clouds, aerosols, and water vapor [55]. As the world's largest developing country, rapid economic development and rapid population growth in China have led to the emission of increasing quantities of man-made aerosols into the atmosphere. Aerosols can simultaneously change the amounts of direct and diffuse radiation reaching the surface [56]. Li et al. [57] reported that radiation decreased by about 24.1 W m^{-2} from September 2004 to September 2005 because of the higher aerosol concentration by using aerosol observation data from the Xianghe Station in China. In addition, volcanic eruptions can

also strongly affect global and diffuse radiation [58,59]. Ren et al. [25] observed that the eruption of Mount Pinatubo in the Philippines in 1991 caused a rapid increase in the amount of diffuse radiation in China in the early 1990s.

The TL-LUE model, which provides a distinct means to investigate the effects of R_d changes on GPP, simulates GPP for sunlit (diffuse and direct radiation) and shaded leaves (diffuse radiation) separately. In the present study, during the period 1981–2012, the average GPP contributed by R_d in China was 5.69 Pg C y^{-1}, which accounted for 74.48% of the total annual GPP. This finding shows that the contribution of R_d to GPP in China was greater than that of direct radiation. The higher contribution of R_d to GPP was largely because of the high fraction of R_d and was also associated with the higher LUE of R_d. The present results showed that the increase in R_d ratio could compensate for the reduction in GPP because of the lower photosynthetically effective radiation. These results will help to quantify the impacts of R_d on GPP and enhance knowledge of the possible causes of carbon budget variation.

Although the mean annual GPP and the GPP of each vegetation type are comparable to those reported by many previous studies (Table 4), some marked differences are apparent. The possible reasons are, first, that model structures are different, not only between process models and LUE models, but also among various LUE models. Second, the modeling area and period are set differently. For example, in the Carnegie-Ames-Stanford approach (CASA) (Table 4), Piao et al. [50] estimated that the total amount of GPP for the period 1982–2009 only varied by 2.66–3.16 Pg C y^{-1}, whereas the average annual GPP reported by Zhu et al. [51] for 1993 was 6.24 Pg C y^{-1}, in which maximum LUE was retrieved based on observations at 690 sites. Third, the types of input data used are inconsistent, covering different time ranges and differing in spatial and temporal resolutions.

Several uncertainties in the present study are acknowledged. First, the R_g of 1981 as a baseline was used to investigate the effect of R_g and diffuse radiation fraction on GPP in terrestrial ecosystems. The advantages of this method were that the annual R_g remained unchanged from 1981 to 2012 and the variation tendency of daily R_g variation to R_g values in 1981 was consistent. However, this method would result in a degree of uncertainty regarding daily R_g. For example, for a year that included many cloudy days, the R_g of a sunny day would be overestimated.

Second, the TL-LUE model has been validated worldwide [42–44], showing that the model performance for GPP simulations is satisfactory. In the present study, we obtained a high R^2 (0.82) value for comparisons between the model-simulated GPP and observed GPP values. However, an extremely limited number of flux sites in China were used to optimize LUE_{sun} and LUE_{shaded} [43], which would cause their underestimation for some ecosystems, especially for crops. Compared with C_3 plants, C_4 plants photosynthesize by the combination of vascular bundle sheath cells and mesophyll cells, which have a higher CO_2 assimilation rate, resulting in higher LUE [60]. Therefore, the inclusion of a few sites dominated by C_4 plants to parameterize the model would result in underestimation of LUE_{sun} and LUE_{shaded} used in the model and the subsequent simulation would underestimate GPP values at some sites in China (Figure 5). Therefore, additional flux tower sites in China should be used to validate the model in the future.

In addition, underestimation of LAI values would result in underestimation of simulated GPP values. For example, the LAI values at the GRASS sites used in the present study were significantly lower than those of the MOD15A2 LAI product (Figure 10), which resulted in underestimation of GPP values at these sites. The GPP uncertainties caused by LAI uncertainties have been investigated and the sensitivity of GPP estimates derived from TL-LUE was lower than that of large-leaf LUE models at the site scale [43]. In the present study, the uncertainties of GPP simulated by the TL-LUE model caused by LAI uncertainties at the national scale were investigated (Figure 10). Overestimation of LAI by 10% would result in GPP overestimation by about 1.2–10%, whereas in most areas with higher LAI the overestimation of GPP was no more than 8%; similarly, underestimation of LAI by 10% would result in GPP overestimation by a similar magnitude to that mentioned above but in the inverse direction (Figure 11).

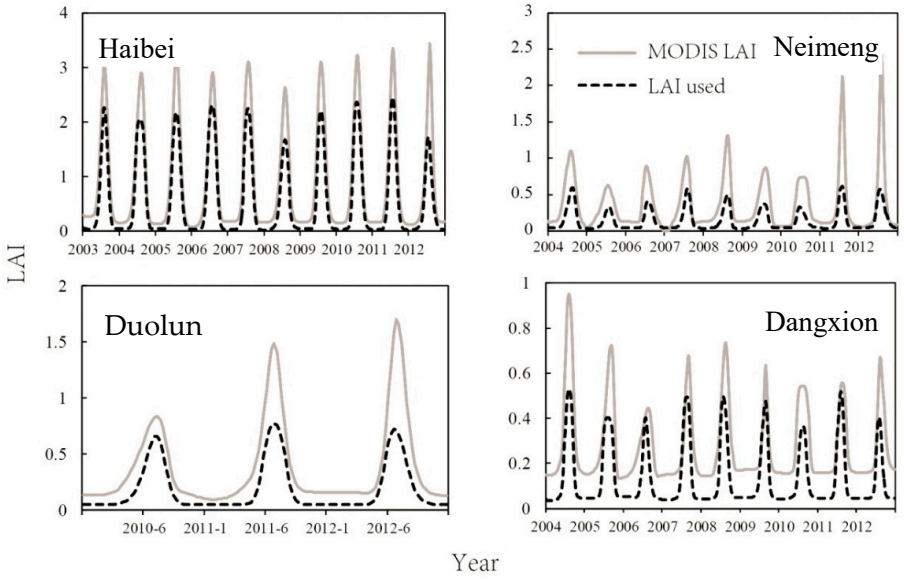

Figure 10. Comparison of leaf area index (LAI) data used in this study and the MODIS LAI product (MOD15A2) for grassland sites, as part of the validation process for estimation of GPP (details for each site were described in Table 3).

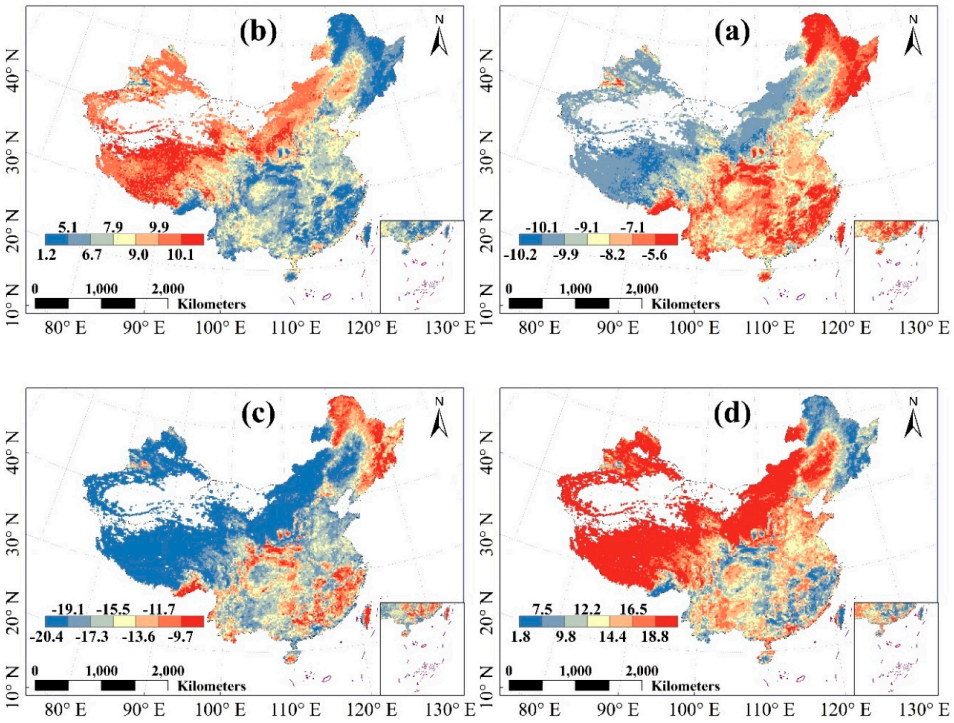

Figure 11. Uncertainties in GPP simulated by the TL-LUE model caused by LAI uncertainties in China during the period 1981–2012 (unit: %). (**a**) Decrease in GPP simulated with the TL-LUE model (GPPTL) caused by a decrease in LAI by 10%; (**b**) increase in GPPTL caused by an increase in LAI by 10%; (**c**) decrease in GPPTL caused by a decrease in LAI by 20% and (**d**) increase in GPPTL caused by an increase in LAI by 20%.

Furthermore, radiation measurements in China are extremely limited, comprising 103 and 81 sites for global radiation and diffuse radiation, respectively; therefore, an interpolation method was used to infer the national-scale R_g and R_d. The Ångström model is commonly used for radiation

interpolation [29,30]. Interpolated radiation data are widely used for ecosystem-level simulations of water and carbon dynamics [44,61]. However, because of the limited available measurements, national R_g and R_d were interpolated to 500 m based on daily extraterrestrial radiation and sunshine duration, omitting many of the drivers of dimming and R_d, which would result in R_d and R_g uncertainties, especially in heterogeneous areas.

5. Conclusions

In this study, we modeled the effects on GPP of solar radiation variation caused by changes in diffuse radiation in China over the period 1981–2012 using a two-leaf light use efficiency model (TL-LUE), which was driven by national global radiation in conjunction with other meteorological data and remotely sensed data. The main findings are as follows:

(i) The annual mean R_g in China significantly decreased over the period 1981–2012 by 2.18 MJ m^{-2} y^{-1}, whereas the diffuse radiation increased. A significant reduction in R_g and increases in the diffuse radiation fraction were observed in the Beijing–Tianjin–Hebei region and on the Qinghai–Tibet Plateau. The annual mean R_d predominantly showed an upward trend over the study period, especially on the southeastern coast and the Qinghai–Tibet Plateau.

(ii) During the period 1981–2012, the average annual total GPP of China's terrestrial ecosystems was 7.64 Pg C y^{-1}, comprising a contribution from R_d of 5.69 Pg C y^{-1}. The total GPP decreased by 0.09 Pg C y^{-1}, although this decrease was partially compensated for by about 50% because of the increase in R_d. Clearly, the increase in LUE of canopy light associated with R_d partly compensated for the reduction in total GPP caused by the reduced R_g in China.

Supplementary Materials: The following are available online at http://www.mdpi.com/2072-4292/12/20/3355/s1, Figure S1: Distribution of sunshine duration, diffuse and global radiation station in China. Figure S2: Observed and interpolated daily global radiation at 12 sites in 2014; Figure S3: Observed and interpolated daily R_d at 12 sites in 2014; Figure S4: Comparisons of estimated R_g and R_d between this study and that of Ren et al. [30]; Figure S5: Spatial distribution of mean annual LAI in China from 1981 to 2012; Table S1: Proportions of sites distributed in different aerosol optical depth (AOD) levels. Table S2: Proportions of sites distributed in different AOD levels. Table S3: Scenario simulations of the impact of radiation change on GPP.

Author Contributions: Conceptualization, W.J.; formal analysis and methodology, X.W.; resources and validation, L.Z., Z.C., Y.L. and Y.S.; writing—original draft preparation, Y.Z.; writing—review and editing, W.H. All authors have read and agreed to the published version of the manuscript.

Funding: This research was funded by the National Key Research and Development Program of China (2016YFA0600202) and by the National Natural Science Foundation of China (42077419).

Conflicts of Interest: The authors declare no conflict of interest.

References

1. Le, Q.C.; Raupach, M.R.; Canadell, J.G.; Marland, G.; Bopp, L.; Ciais, P.; Conway, T.J.; Doney, S.C.; Feely, R.A.; Foster, P.; et al. Trends in the sources and sinks of carbon dioxide. *Nat. Geosci.* **2009**, *2*, 831–836.
2. Yuan, W.P.; Cai, W.W.; Xia, J.Z. Global comparison of light use efficiency models for simulating terrestrial vegetation gross primary production based on the LaThuile database. *Agric. For. Meteorol.* **2014**, *192–193*, 108–120. [CrossRef]
3. Kanniah, K.D.; Beringer, J.; North, P.; Hutley, L. Control of atmospheric particles on diffuse radiation and terrestrial plant productivity: A review. *Progr. Phys. Geogr.* **2012**, *36*, 209–237. [CrossRef]
4. Cohan, D.S.; Xu, J.; Greenwald, R.; Bergin, M.H.; Chameides, W.L. Impact of atmospheric aerosol light scattering and absorption on terrestrial net primary productivity. *Glob. Biogeochem. Cycle* **2002**, *16*, 37. [CrossRef]
5. Mercado, L.M.; Bellouin, N.; Sitch, S.; Boucher, O.; Huntingford, C.; Wild, M.; Cox, P.M. Impact of changes in diffuse radiation on the global land carbon sink. *Nature* **2009**, *458*, 1014–1017. [CrossRef] [PubMed]
6. Farquhar, G.D.; Roderick, M.L. Pinatubo diffuse light and the carbon cycle. *Science* **2003**, *299*, 1997–1998. [CrossRef]

7. Gu, L.H.; Fuentes, J.D.; Shugart, H.H.; Staebler, R.M.; Black, T.A. Responses of net ecosystem exchanges of carbon dioxide to changes in cloudiness: Results from two North American deciduous forest. *J. Geophys. Res.* **1999**, *104*, 31421–31434. [CrossRef]
8. Gu, L.H.; Baldocchi, D.; Verma, S.B.; Black, T.A.; Vesala, T.; Falge, E.M.; Dowty, P.R. Advantages of diffuse radiation for terrestrial ecosystem productivity. *J. Geophys. Res.* **2002**, *107*, ACL2-1–ACL2-23. [CrossRef]
9. Gu, L.H.; Baldocchi, D.D.; Wofsy, S.C.; Munger, J.W.; Michalsky, J.J.; Urbanski, S.P.; Boden, T.A. Response of a deciduous forest to the mount Pinatubo eruption: Enhanced photosynthesis. *Science* **2003**, *299*, 2035–2038. [CrossRef]
10. Black, K.; Davis, P.; Lynch, P.; Jones, M.; McGettigan, M.; Osborne, B. Long-term trends in solar irradiance in ireland and their potential effects on gross primary productivity. *Agric. For. Meteorol.* **2006**, *141*, 118–132. [CrossRef]
11. Chen, M.; Zhuang, Q.L. Evaluating aerosol direct radiative effects on global terrestrial ecosystem carbon dynamics from 2003 to 2010. *Tellus B* **2014**, *66*, 21808. [CrossRef]
12. He, M.Z.; Ju, W.M.; Zhou, Y.L.; Chen, J.M.; He, H.L.; Wang, S.Q.; Wang, H.M.; Guan, D.X.; Yan, J.H.; Li, Y.N.; et al. Development of a two-leaf light use efficiency model for improving the calculation of terrestrial gross primary production. *Agric. For. Meteorol.* **2013**, *173*, 28–39. [CrossRef]
13. Wang, S.Q.; Huang, K.; Yan, H.; Yan, H.M.; Zhou, L.; Wang, H.M.; Zhang, J.H.; Yan, J.H.; Zhao, L.; Wang, Y.F.; et al. Improving the light use efficiency model for simulating terrestrial vegetation gross primary production by the inclusion of diffuse radiation across ecosystems in China. *Ecol. Complex.* **2015**, *23*, 1–13. [CrossRef]
14. Wang, S.; Ibrom, A.; Bauer-Gottwein, P.; Garcia, M. Incorporating diffuse radiation into a light use efficiency and evapotranspiration model: An 11-year study in a high latitude deciduous forest. *Agric. For. Meteorol.* **2018**, *248*, 479–493. [CrossRef]
15. Yan, H.; Wang, S.Q.; da Rocha, H.R.; Rap, A.; Bonal, D.; Butt, N.; Coupe, N.R.; Shugart, H.H. Simulation of the unexpected photosynthetic seasonality in Amazonian evergreen forests by using an improved diffuse fraction-based light use efficiency model. *J. Geophys. Res. Biogeosci.* **2017**, *122*, 3014–3030. [CrossRef]
16. Zheng, Y.; Shen, R.Q.; Wang, Y.W.; Li, X.Q.; Liu, S.G.; Liang, S.L.; Chen, J.M.; Ju, W.M.; Zhang, L.; Yuan, W.P. Improved estimate of global gross primary production for reproducing its long-term variation, 1982–2017. *Earth Syst. Sci. Data* **2019**, *126*, 1–31.
17. Wild, M.; Gilgen, H.; Roesch, A.; Ohmura, A.; Long, C.N.; Dutton, E.G.; Forgan, B.; Kallis, A.; Russak, V.; Tsvetkov, A. From dimming to brightening: Decadal changes in solar radiation at earth's surface. *Science* **2005**, *308*, 847–850. [CrossRef]
18. Ohmura, A. Observed long-term variations of solar irradiance at the earth's surface. *Space Sci. Rev.* **2006**, *125*, 111–128. [CrossRef]
19. Shi, G.Y.; Hayasaka, T.; Ohmura, A.; Chen, Z.H.; Wang, B.; Zhao, J.Q.; Che, H.Z.; Xu, L. Data quality assessment and the long-term trend of ground solar radiation in China. *J. Appl. Meteor.* **2008**, *47*, 1006–1016. [CrossRef]
20. Norris, J.R.; Wild, M. Trends in aerosol radiative effects over China and Japan inferred from observed cloud cover solar "dimming" and solar "brightening". *J. Geophys. Res.* **2009**, *114*, D15. [CrossRef]
21. Qi, Y.; Fang, S.B.; Zhou, W.Z. Variation and spatial distribution of surface solar radiation in China over recent 50 years. *Acta Ecol. Sin.* **2014**, *34*, 7444–7453. (In Chinese)
22. Che, H.Z.; Shi, G.Y.; Zhang, X.Y.; Arimoto, R.; Zhao, J.Q.; Xu, L.; Wang, B.; Chen, Z.H. Analysis of 40 years of solar radiation data from China, 1961–2000. *Geophys. Res. Lett.* **2005**, *32*, 2341–2352. [CrossRef]
23. Qian, Y.; Kaiser, D.P.; Leung, L.R.; Xu, M. More frequent cloud-free sky and less surface solar radiation in China from 1955 to 2000. *Geophys. Res. Lett.* **2006**, *33*, L01812. [CrossRef]
24. Yang, H.B.; Yang, D.W. Climatic factors influencing changing pan evaporation across China from 1961 to 2001. *J. Hydrol.* **2012**, *414–415*, 184–193. [CrossRef]
25. Ren, X.L.; He, H.L.; Zhang, L.; Zhou, L.; Yu, G.R.; Fan, J.W. Spatiotemporal variability analysis of diffuse radiation in China during 1981–2010. *Ann. Geophys.* **2013**, *31*, 277–289. [CrossRef]
26. He, X.Z.; Zhou, T.; Jia, G.S.; Zhang, Z.Y.; Li, X.J.; Zhao, C.; Feng, S.H. Modeled effects of changes in the amount and diffuse fraction of PAR on forest GPP. *J. Nat. Res.* **2011**, *26*, 619–634.

27. Li, D.Q.; Zhou, Y.L.; Ju, W.M.; Wang, H.M.; Liu, Y.B.; Wu, X.C. Modelling the effects of changes in solar radiation on gross primary production in subtropical evergreen needle-leaf plantations. *Chin. J. Plant Ecol.* **2014**, *38*, 219–230.
28. Allen, R.G.; Walter, I.A.; Elliott, R.L.; Howell, T.A.; Itenfisu, D.; Jensen, M.E.; Snyder, R.L. *The ASCE Standardized Reference Evapotranspiration Equation*; Final Report; Environmental and Water Resources Institute of the American Society of Civil Engineers: Reston, VA, USA, 2005.
29. Ångström, A. Solar and terrestrial radiation. Report to the international commission for solar research on actinometric investigations of solar and atmospheric radiation. *Q. J. R. Meteorol. Soc.* **1924**, *50*, 121–126. [CrossRef]
30. Ren, X.L.; He, H.L.; Zhang, L.; Yu, G.R. Global radiation, photosynthetically active radiation, and the diffuse component dataset of China, 1981–2010. *Earth Syst. Sci. Data* **2018**, *10*, 1217–1226. [CrossRef]
31. Chen, R.S.; Ersi, K.; Yang, J.P.; Lu, S.H.; Zhao, W.Z. Validation of five global radiation models with measured daily data in China. *Energy Conv. Manag.* **2004**, *45*, 1759–1769. [CrossRef]
32. Roderick, M.L. Estimating the diffuse component from daily and monthly measurements of global radiation. *Agric. For. Meteorol.* **1999**, *95*, 169–185. [CrossRef]
33. Singh, U.P. Diffuse Radiation Calculation Methods. Ph.D. Thesis, Science Arizona State University, Tempe, AZ, USA, 2016.
34. Liu, Y.; Liu, R.G.; Chen, J.M. Retrospective retrieval of long-term consistent global leaf area index (1981–2011) from combined AVHRR and MODIS data. *J. Geophys. Res.* **2012**, *117*, G04003. [CrossRef]
35. Sawada, Y.; Koike, T. Simultaneous estimation of both hydrological and ecological parameters in an ecohydrological model by assimilating microwave signal. *J. Geophys. Res. Atmos.* **2014**, *119*, 8839–8857. [CrossRef]
36. Gao, Y.; Zhu, X.J.; Yu, G.R.; He, N.P.; Wang, Q.F.; Tian, J. Water use efficiency threshold for terrestrial ecosystem carbon sequestration in China under afforestation. *Agric. For. Meteorol.* **2014**, *195–196*, 32–37. [CrossRef]
37. Zhu, X.J.; Yu, G.R.; He, H.L.; Wang, Q.F.; Chen, Z.; Gao, Y.N.; Zhang, Y.P.; Zhang, J.H.; Yan, J.H.; Wang, H.M.; et al. Geographical statistical assessments of carbon fluxes in terrestrial ecosystems of China: Results from upscaling network observations. *Glob. Planet. Chang.* **2014**, *118*, 52–61. [CrossRef]
38. Piao, S.L.; Yin, G.D.; Tan, J.G.; Cheng, L.; Huang, M.T.; Li, Y.; Liu, R.G.; Mao, J.F.; Myneni, R.B.; Peng, S.S.; et al. Detection and attribution of vegetation greening trend in China over the last 30 years. *Glob. Chang. Biol.* **2015**, *21*, 1601–1609. [CrossRef]
39. Chen, J.M.; Ju, W.M.; Ciais, P.; Viovy, N.; Liu, R.G.; Liu, Y.; Lu, X.H. Vegetation structural change since 1981 significantly enhanced the terrestrial carbon sink. *Nat. Commun.* **2019**, *10*, 1–7. [CrossRef]
40. Running, S.; Thornton, P.; Nemani, R.; Glassy, J. Global terrestrial gross and net primary productivity from the earth observing system. *Methods Ecosyst. Sci.* **2000**, *3*, 44–57.
41. Chen, J.M.; Liu, J.; Cihlar, J.; Goulden, M.L. Daily canopy photosynthesis model through temporal and spatial scaling for remote sensing applications. *Ecol. Modell.* **1999**, *124*, 99–119. [CrossRef]
42. Wu, X.C.; Ju, W.M.; Zhou, Y.L.; He, M.Z.; Law, B.E.; Black, T.A.; Margolis, H.A.; Cescatti, A.; Gu, L.H.; Montagnani, L.; et al. Performance of linear and nonlinear two-leaf light use efficiency models at different temporal scales. *Remote Sens.* **2015**, *7*, 2238–2278. [CrossRef]
43. Zhou, Y.L.; Wu, X.C.; Ju, W.M.; Chen, J.M.; Wang, S.Q.; Yuan, W.P.; Black, T.A.; Jassal, R.; Ibrom, A.; Han, S.J.; et al. Global parameterization and validation of a two-leaf light use efficiency model for predicting gross primary production across FLUXNET sites. *J. Geophys. Res. Biogeosci.* **2016**, *121*, 1045–1072. [CrossRef]
44. Zan, M.; Zhou, Y.L.; Ju, W.M.; Zhang, Y.G.; Zhang, L.M.; Liu, Y.B. Performance of a two-leaf light use efficiency model for mapping gross primary productivity against remotely sensed sun-induced chlorophyll fluorescence data. *Sci. Total Environ.* **2018**, *613–614*, 977–989. [CrossRef]
45. Tang, W.J.; Yang, K.; Qin, J.; Cheng, C.C.K.; He, J. Solar radiation trend across China in recent decades: A revisit with quality-controlled data. *Atmos. Chem. Phys.* **2011**, *11*, 393–406. [CrossRef]
46. Lin, C.G.; Wu, H.P.; Ou, T.H.; Chen, D.L. A new perspective on solar dimming over the Tibetan Plateau. *Int. J. Climatol.* **2019**, *39*, 302–316. [CrossRef]
47. Li, X.L.; Liang, S.L.; Yu, G.R.; Yuan, W.P.; Cheng, X.; Xia, J.Z.; Zhao, T.B.; Feng, J.M.; Ma, Z.G.; Ma, M.G.; et al. Estimation of gross primary production over the terrestrial ecosystems in China. *Ecol. Modell.* **2013**, *261–262*, 80–92. [CrossRef]

48. Wang, Q.F.; Zheng, H.; Zhu, X.J.; Yu, G.R. Primary estimation of Chinese terrestrial carbon sequestration during 2001–2010. *Sci. Bull.* **2015**, *60*, 577–590. [CrossRef]
49. Gao, Z.Q.; Liu, J.Y. Comparative study on net productivity of vegetation in China. *Chin. Sci. Bull.* **2008**, *53*, 317–326. [CrossRef]
50. Piao, S.L.; Fang, J.Y.; Zhou, L.M.; Zhu, B.; Tan, K.; Tao, S. Changes in vegetation net primary productivity from 1982 to 1999 in China. *Glob. Biogeochem. Cycle* **2005**, *19*, GB2027. [CrossRef]
51. Zhu, W.Q.; Pan, Y.Z.; Zhang, J.S. Estimation of net primary productivity of Chinese terrestrial vegetation based on remote sensing. *Acta Phytoecol. Sin.* **2007**, *31*, 413–424. (In Chinese)
52. Feng, X.; Liu, G.H.; Chen, J.; Chen, M.; Liu, J.; Ju, W.M.; Sun, R.; Zhou, W. Net primary productivity of China's terrestrial ecosystems from a process model driven by remote sensing. *J. Environ. Manag.* **2007**, *85*, 563–573. [CrossRef]
53. Xiao, X.; Melillo, J.M.; Kicklighter, D.W.; Pan, Y.; McGuire, A.D.; Helfrich, J. Net primary production of terrestrial ecosystems in China and its equilibrium responses to changes in climate and atmospheric CO_2 concentration. *Acta Phytoecol. Sin.* **1998**, *22*, 97–118.
54. Tao, B.; Li, K.R.; Shao, X.M.; Cao, M.K. The temporal and spatial patterns of terrestrial net primary productivity in China. *J. Geogr. Sci.* **2003**, *13*, 163–171.
55. Stanhill, G.; Cohen, S. Global dimming: A review of the evidence for a widespread and significant reduction in global radiation with discussion of its possible causes and possible agricultural consequences. *Agric. For. Meteorol.* **2001**, *107*, 255–278. [CrossRef]
56. Ramanathan, V.; Crutzen, P.J.; Kiehl, J.T. Atmosphere, aerosols, climate, and the hydrological cycle. *Science* **2001**, *294*, 2119–2124. [CrossRef]
57. Li., Z.; Xia, X.; Cribb, M. Aerosol optical properties and their radiative effects in northern China. *J. Geophys. Res. Atmos.* **2007**, D22S01. [CrossRef]
58. Qiu, J.H.; Yang, L.Q. Variation characteristics of atmospheric aerosol optical depths and visibility in North China during 1980–1994. *Atmos. Environ.* **2000**, *34*, 603–609.
59. Wild, M.; Trüssel, B.; Ohmura, A. Global dimming and brightening: An update beyond 2000. *J. Geophys. Res.* **2009**, *114*. [CrossRef]
60. Hicks, S.R.A.; Brisk, D.D.; Call, C.A. Co-existence of a perennial C3 bunchgrass in a C4 dominated grassland: An evaluation of gas exchange characteristics. *Photosynthetica* **1990**, *24*, 63–74.
61. Liu, Y.B.; Xiao, J.F.; Ju, W.M.; Zhu, G.L.; Wu, X.C.; Fan, W.L.; Li, D.Q.; Zhou, Y.L. Satellite-derived LAI products exhibit large discrepancies and can lead to substantial uncertainty in simulated carbon and water fluxes. *Remote Sens. Environ.* **2018**, *206*, 174–188. [CrossRef]